A low-order model for wind farm control

Jennifer Annoni and Peter Seiler

***Abstract*— Wind turbines in a wind farm are operated individually to maximize their own power regardless of the impact of aerodynamic interactions on neighboring turbines. There is the potential to increase power and reduce overall structural loads by properly coordinating the turbines. To perform control design and analysis, a model needs to be of low computational complexity but retain the necessary dynamics seen in high-fidelity models. This paper addresses a model reduction approach that computes the dominant modes of the flow that capture the energy and frequency characteristics of the system. Specifically, the paper uses the balanced proper orthogonal decomposition technique to construct the dominant input/output modes. Using these modes, a low-order model of a wind farm is constructed that can be used for control design.**

I. Introduction

In the United States, many states have a Renewable Portfolio Standard (RPS) or Goal. For example, Minnesota has a RPS target of 25% renewable energy by 2025 [1]. Wind energy will be a significant factor in achieving this goal. As suitable land for wind farm development decreases, wind energy will need to become more efficient. Wind farm control can be used to increase wind energy efficiency by maximizing power in wind farms that are already installed. It can also be used to mitigate structural loads to maximize the lifetime of the turbines and better integrate wind energy into the energy market. Performing wind farm control requires an understanding of the aerodynamic interactions in a wind farm. Some studies have been done to understand the turbulent structures generated behind the turbines [2], [3], [4]. These turbulent structures propagate downstream and affect the overall power output and the structural loads on downstream turbines.

Currently, turbines in a wind farm are operated to maximize their own performance. Many studies have been done showing that operating all turbines at their optimal operating point leads to sub-optimal performance. Implementing coordinated wind farm control strategies has the potential to increase the overall performance of a wind farm [5], [6], [7], [8], [9], [10], [11]. A variety of wake models exist in literature that are useful for studying wind farm control. The simplest models are the Park model [12] and the eddy viscosity model [13]. These models provide a quick, preliminary description of the wake interactions in a wind farm. Several high fidelity CFD models have been developed as well, including [14], [15]. These high fidelity models are more accurate tools and can be used for evaluating wind farm controllers. However, they are computationally expensive.

In literature, low- and high-fidelity models have been used to evaluate wind farm control strategies. The analysis provides conflicting results based on the wake model chosen for control design. For example, control strategies using simple static models often report significant improvements in wind farm performance [8]. However, an analysis of similar control strategies using high fidelity simulations results in minimal to no improvement in wind farm performance [16].

This paper addresses a way to take advantage of the knowledge of aerodynamic interactions in a wind farm gathered from high-fidelity simulations or field experiments to construct low-order models that can be used for control. For simplicity, this paper will use a medium-fidelity model, described in Section II, to highlight some of the advantages of this approach with the intention of extending this work to high-fidelity models in future work. Section III describes two existing techniques to characterize the dominant structures in the flow field: proper orthogonal decomposition (POD) and balanced POD (BPOD). Both techniques have been widely used in the fluids literature [17], [18]. The POD technique focuses on the overall flow field and has been recently applied to wind farm dynamics [19] to obtain a low-order approximation of the flow field. BPOD focuses on retaining modes of the flow that have the dominant effect from a specific input(s) to a specific output(s). Section III-C uses BPOD to construct a low-order model that approximates the dynamics and input/output characteristics of a wind farm. The results of this low-order model are presented in Section IV. Finally, conclusions and suggestions for future work are given in Section V.

II. Actuator Disk Model

A. Wind Farm Setup

Consider a wind farm with N number of turbines located on an arbitrary grid with arbitrary locations defined by (x_i, y_i) where i refers to the turbine i in the wind farm. Each turbine has an input axial induction factor, a_i. The axial induction for a single turbine is defined as $a := 1 - \frac{u_1}{U_{in}}$, where u_1 denotes the average horizontal speed across the rotor plane, and U_{in} denotes the average inflow velocity. In addition, the power of each turbine can be measured, P_i. The power generated by each turbine depends on the inflow wind speed as well as the axial induction factor. The power captured from turbine i, P_i $[W]$, is given by:

$$P_i = \frac{1}{2}\rho A u_i^3 C_{P,i} \tag{1}$$

where ρ [kg/m^3] is the air density, A [m] is the area swept by the rotor, u_i [m/s] is the wind speed perpendicular to the rotor plane, and $C_{P,i}$ is the power coefficient, which is a function of the axial induction factor [20]:

$$C_{P,i} = 4a_i(1-a_i)^2 \tag{2}$$

Individual turbines typically try to maximize their own power by operating at an optimal axial induction factor. The optimal induction factor corresponding to the optimal power coefficient is $a = \frac{1}{3}$. Additional details and references about single turbine control can be found in [8], [21], [20].

The turbines operating at the front of the wind farm disturb the flow through the wind farm and this impacts turbines operating downstream. The wind farm control problem can be thought of as a multi-input, multi-output system where the axial induction factors at each turbine would be the inputs and the power measured at each turbine would be the outputs. By properly coordinating the turbines in a wind farm, there is the potential to maximize power and reduce overall structural loads. A few control strategies have been investigated including yaw control and axial-induction-based control. This paper focuses on the modeling aspects and does not include details on a specific control strategy. More information can be found in [7], [8], [22], [23]. The effective design and analysis of such control strategies require wake models of sufficient accuracy but low computational complexity. The remainder of this paper will address the development of a low-order model suitable for control.

B. Governing Equations

The actuator disk model is considered in this paper [24], [25]. This model solves the 2D unsteady, incompressible, Reynolds Averaged Navier-Stokes (RANS) equations. The typical operating wind speeds in a wind farm do not exceed 25 m/s. This is low relative to the speed of sound at sea level ($\sim$300 m/s) and hence it is sufficient to assume incompressibility [26]. Let (u, v) denote the streamwise and spanwise velocity components and (x, y) denote the downstream and spanwise distances. The streamwise and spanwise components are decomposed, using the Reynolds decomposition, into $u = \langle U\rangle + u^{'}$ and $v = \langle V\rangle + v^{'}$, where $\langle U\rangle$ and $\langle V\rangle$ are the Reynolds averages and $u^{'}$ and $v^{'}$ are the fluctuations. The RANS governing equations are:

$$\frac{\partial\langle U\rangle}{\partial x} + \frac{\partial\langle V\rangle}{\partial y} = 0 \tag{3}$$

$$\begin{aligned}\frac{\partial\langle U\rangle}{\partial t} + \langle U\rangle\frac{\partial\langle U\rangle}{\partial x} + \langle V\rangle\frac{\partial\langle U\rangle}{\partial y} &= -\frac{1}{\rho}\frac{\partial\langle P\rangle}{\partial x} \\ \nu\left(\frac{\partial^2\langle U\rangle}{\partial x^2} + \frac{\partial^2\langle U\rangle}{\partial y^2}\right) &+ \frac{\partial\langle u^{'}v^{'}\rangle}{\partial y} + \frac{\langle u^{'2}\rangle}{\partial x} + f_x\end{aligned} \tag{4}$$

$$\begin{aligned}\frac{\partial\langle V\rangle}{\partial t} + \langle U\rangle\frac{\partial\langle V\rangle}{\partial x} + \langle V\rangle\frac{\partial\langle V\rangle}{\partial y} &= -\frac{1}{\rho}\frac{\partial\langle P\rangle}{\partial x} + \\ \nu\left(\frac{\partial^2\langle V\rangle}{\partial x^2} + \frac{\partial^2\langle V\rangle}{\partial y^2}\right) &+ \frac{\partial\langle u^{'}v^{'}\rangle}{\partial x} + \frac{\langle v^{'2}\rangle}{\partial y}\end{aligned} \tag{5}$$

where ν [m^2/s] is the kinematic viscosity and f_x [N/m^3] is a volume force on the turbine in the x direction. The Reynolds stresses, specifically $\langle u^{'2}\rangle$, $\langle u^{'}v^{'}\rangle$, and $\langle v^{'2}\rangle$, are present in turbulent flows. These terms cause the diffusion of momentum normal to the flow direction and enhance the viscous effects in the flow. This mixing causes the wake to recover more quickly downstream of the turbine. There are various ways to model this stress. For simplicity, the mixing length hypothesis is used to model these Reynolds stresses [26].

The loading of each turbine is defined linearly. Specifically, assume that all spatial units have been nondimensionalized by the turbine diameter D. If the hub of the upstream turbine i is placed at $x = x_i$ and $y = y_i$ then the rotor plane lies within $y_i - \frac{1}{2} \le y \le y_i + \frac{1}{2}$. The forcing term introduced by the turbines is then given by:

$$f_x(x,y,t) := \begin{cases} kC_{T,i}(t)|y-y_i| & \text{if } x = x_i \ \&\ |y-y_i| \le 0.5 \\ 0 & \text{else} \end{cases} \tag{6}$$

where $k := \rho A U_{in}^2$ and $C_{T,i}$ is the thrust coefficient of the turbine i. The thrust coefficient for each turbine is a function of the axial induction factor and is defined as $C_{T,i}(t) = 4a_i(t)(1-a_i(t))$ where $a_i(t)$ is the time varying single input to the turbine i. This linear profile is smallest at the rotor hub and grows linearly at the blade tips. The loading magnitude, as specified by the input $a_i(t)$, can be changed on a real turbine via blade pitch or changing the tip speed ratio via generator torque control [20], [27].

These equations are solved using standard CFD methods [28]. The grid is defined by N_x points in the streamwise x direction and N_y point in the spanwise y direction. Typically, for this actuator disk model, the spacing between grid points is $\delta x = 0.05$ and $\delta y = 0.05$ with a time step of $\delta t = 0.01$. Fig. 1 and 2 show an example of a 4×4 wind farm where mean streamwise and spanwise velocity are computed for the actuator disk model. In these figures, the turbines are separated by $3D$ in the spanwise y direction and $4D$ in the streamwise x direction. The velocities are normalized by U_∞.

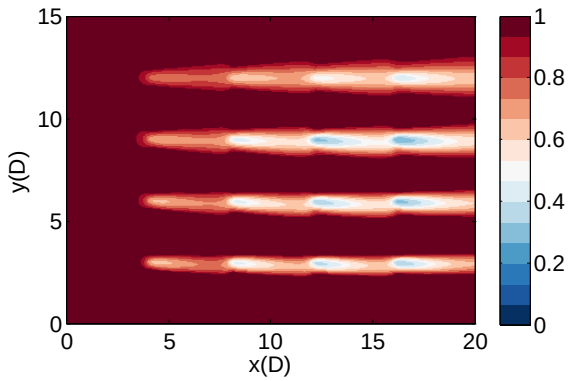

Fig. 1. Mean streamwise velocity computed using the actuator disk model for a 4×4 wind farm with $3D$ spacing in the y direciton and $4D$ spacing in the x direction

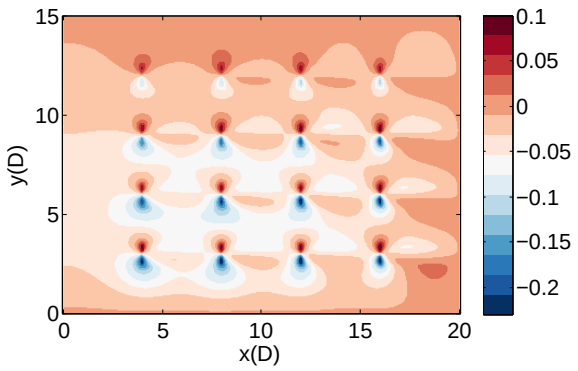

Fig. 2. Mean spanwise velocity computed using the actuator disk model for a 4×4 wind farm with $3D$ spacing in the y direciton and $4D$ spacing in the x direction

The boundary conditions of this model are:

$$\begin{aligned} u(x=0,y,t) = u(x,y=0,t) = u(x,y=L,t) = U_\infty \\ v(x=0,y,t) = v(x,y=0,t) = v(x,y=L,t) = 0 \end{aligned} \tag{7}$$

where L is the total spanwise distance. In this example, $L =$ 14D, the kinematic viscosity is $\nu = 1.461 \times 10^{-5}$ m^2/s, and $U_\infty = 8$ m/s.

Note the turbines are modeled as actuator disks. The wakes directly behind real turbines are dominated by tip vortices that are generated based on the blade geometry. The blades are not modeled in this simulation and as a result, this model cannot accurately depict this near wake region. However, this model captures the effects of the flow far downstream, greater than $3D$, where the flow is less dependent on turbine geometry. Therefore, this model is useful for studying the far wake of a turbine in steady and unsteady flows. It should be noted that changing wind speed and direction are not addressed in this paper. Possible approaches include running multiple simulations and developing controllers to be gain scheduled in a similar manner as is done at the single turbine level [29]. Additional work is being done in this area.

C. Linearized Equations

The first step in producing a model suitable for controls is to linearize the equations of the actuator disk model. For the purposes of this paper, the actuator disk equations will be linearized around a base flow of $\mathbf{U} = (U(x,y), V(x,y), 0)$ where $U(x,y)$ and $V(x,y)$ define the baseflow that corresponds to all turbines operating at their peak efficiency.

The linearized governing equations about the baseflow, after some algebraic manipulation, can be rewritten as:

$$\frac{\partial}{\partial t}\begin{bmatrix} u' \\ v' \end{bmatrix} = A \begin{bmatrix} u' \\ v' \end{bmatrix} + Ba(t) \tag{8}$$

where $u' \in \mathbb{R}^{(N_x \times N_y)\times 1}$ denotes the fluctuations from the baseflow in the streamwise direction, $v' \in \mathbb{R}^{(N_x \times N_y)\times 1}$ denotes the fluctuations from the baseflow in the spanwise direction, $A \in \mathbb{R}^{(2\times N_x \times N_y)\times(2\times N_x \times N_y)}$ contains the discretization information of the flow field, $B \in \mathbb{R}^{(2\times N_x \times N_y)\times N_{turb}}$ contains the location of the turbines, and $a(t) \in \mathbb{R}^{N_{turb}\times 1}$ is the input to the turbines with N_{turb} denoting the number of inputs, which in this case is the number of turbines. The power, P_i, at each turbine is measured, recall (1).

Linearizing (1), the measurement equation can be rewritten as:

$$P = \begin{bmatrix} C & 0 \end{bmatrix} \begin{bmatrix} u' \\ v' \end{bmatrix} + Da(t) \tag{9}$$

where $C \in \mathbb{R}^{N_{turb}\times(N_x \times N_y)}$ contains the locations of the measurements with N_{turb} number of outputs, and $D \in \mathbb{R}^{N_{turb}\times N_{turb}}$ contains information about the turbine efficiency. More details on the linearization can be found in [30]. In this representation, the linearized system is given by a dynamic system of the form:

$$\begin{aligned} \dot{x} &= Ax + Ba \\ y &= Cx + Da \end{aligned} \tag{10}$$

where $x := \begin{bmatrix} u' \\ v' \end{bmatrix}$. This linearized model contains $2\times N_x \times N_y$ states and is not suitable for control design and analysis. The model reduction techniques described in the next section can be used to obtain a low-order model of the wind farm.

III. Model Reduction Formulation

A. Proper Orthogonal Decomposition

Proper orthogonal decomposition (POD) provides a low-order approximation that captures the dominant turbulent structures in the flow. Specifically, POD can be used to extract dominant spatial features from both simulation and experimental data that can be used to dynamically reconstruct the structures in a flow field [17]. This can be done by projecting the velocity field on to a set of orthogonal basis functions. A projection matrix is constructed to minimize the error between the full and reduced order systems:

$$\int_0^{T_{max}} \|x(t) - P_r x(t)\|^2 \, dt \tag{11}$$

where T_{max} is the total simulation time, $x(t)$ is the simulated variable, and P_r is the projection matrix. The projection matrix can be defined in terms of the basis functions:

$$P_r = \sum_{k=1}^{r} \varphi_k \varphi_k^* \tag{12}$$

where φ_k are the POD modes and r represents the reduced order of the system. The eigenfunctions of the flow field are shown to produce the optimal projection that minimizes the total error between the full system and the reduced order system. See [17], [31], [32], [33] for more details.

The computed POD modes can be used to reconstruct the flow using the Galerkin projection [17]. This projection uses a separation of variables approach where the flow field variable can be defined as:

$$u(\mathbf{x},t) = \sum_{j=1}^{r} b_j(t)\varphi_j(\mathbf{x}) \tag{13}$$

where b are the temporal coefficients. In this way, the system (4) and (5) can be rewritten as an ordinary differential equation:

$$\dot{b}_k = \sum_{i=1}^{r}\sum_{j=1}^{r} b_i b_j Q_{ijk} + \sum_{i=1}^{r} b_i D_{ik} + c_k + f_x^{'} \tag{14}$$

where Q represents the nonlinear terms in the flow field u, D represents the linear terms, c represents the constant terms, and $f_x^{'}$ represents the fluctuations in the forcing term in the x direction. The matrices, Q and D, are made up of the POD modes. Detailed expressions of these matrices can be found in [34]. In this way, a set of POD modes can be used to approximately describe the evolution of the flow field [31]. POD modes are good at representing specific datasets. However, POD modes do not necessarily provide a good description of a dynamically evolving flow driven by a forcing input.

B. Balanced Truncation

POD tries to capture the energy in the flow with a small number of modes. A more relevant objective for wind farm control is to capture the most relevant flow dynamics that connect the upstream turbine input to the downstream turbine output. A typical model reduction approach is known as balanced truncation [35], [36], [37]. Consider the linearized actuator disk model (10). To perform balanced truncation on this problem, the controllability and observability gramians need to be computed to understand the influence of the states on the inputs and outputs of the system. Specifically, the controllability gramian specifies the minimum control energy required to reach any specific state. States that require less energy to reach are more controllable and hence have a greater influence on the input/output dynamics. Similarly, the observability gramian specifies the energy in the output measurement when the system evolves from a given initial state (with zero input). States that produce more energy in the output are more observable and hence have a greater influence on the input/output dynamics. The gramians can be computed by solving the Lyapunov equations:

$$\begin{aligned} AW_c + W_c A^* + BB^* = 0 \\ A^* W_o + W_o A + C^* C = 0 \end{aligned} \tag{15}$$

where W_c is the controllability gramian and W_o is the observability gramian.

The gramians are defined by specific coordinates. These coordinates define in which directions the strongest states are aligned. The controllability and observability gramians can have different coordinates. This makes it difficult to choose states to retain since a state may be strongly observable, but not controllable and vice versa. A transformation can be applied to align the properties of the controllability and observability gramians, which allows you to retain states that are strongly controllable and/or observable. A coordinate transformation T can be constructed to diagonalize both the controllability and observability gramians:

$$T^{-1} W_c (T^{-1})^* = T^* W_o T = \Sigma = diag(\sigma_1, ..., \sigma_n) \tag{16}$$

where σ are the Hankel singular values that are independent of the coordinate transformation. Under this transformed system, the states that are significantly influenced by the inputs are also the states that have a significant impact on the outputs. However, this approach becomes intractable for large systems as it requires the solution of the two Lyapunov equations (15). See additional details in [37] and [38].

C. Balanced Proper Orthogonal Decomposition

The combination of POD modes and balanced truncation can be used to implement a method known as balanced proper orthogonal decomposition (BPOD) [31], [32], [33]. Consider the linearized actuator disk system (10). The solution $x(t)$ is found by solving $\dot{x} = Ax$ where the inputs have been set to 0. The initial conditions are defined as the columns of B. This system will be referred to as the forward system for the remainder of this paper.

In addition to computing the solution for the forward system, the solution to the adjoint system can be found by integrating the system:

$$\dot{z} = A^* z \tag{17}$$

with the initial conditions defined as the columns of C. Again, in the case of the two-turbine example, there is only one output, i.e. $z(0) = C^T$. Physically, the adjoint system is used to evaluate the sensitivity of the system due to some perturbation [39], [40], [41], [42].

Using the solutions, $x(t)$ and $z(t)$, the data matrices are formed with the snapshots gathered in the simulations.

$$\begin{aligned} X &= [x(t_1), x(t_2), ..., x(t_m)] \\ Y &= [z(t_1), z(t_2), ..., z(t_m)] \end{aligned} \tag{18}$$

where m is the number of snapshots. At this point, the BPOD modes can be computed from the singular value decomposition of Y^*X:

$$Y^* X = \begin{bmatrix} U_1 & U_2 \end{bmatrix} \begin{bmatrix} \Sigma_1 & 0 \\ 0 & \Sigma_2 \end{bmatrix} \begin{bmatrix} V_1 \\ V_2 \end{bmatrix} \tag{19}$$

where Σ_1 is a matrix $(r \times r)$ and r is the reduced order of the system. The transformation matrices, T and S, can be defined as:

$$\begin{aligned} T &= X V_1 \Sigma_1^{-\frac{1}{2}} \\ S &= \Sigma_1^{-\frac{1}{2}} U_1^* Y^* \end{aligned} \tag{20}$$

The reduced order system is now:

$$\dot{x}_r = SATx + SBf$$
$$y = CT \tag{21}$$

Note the X and Y matrices are $n \times m$ matrices where n is the state dimension, which is typically very large, i.e. tens of thousands or more, while m is the number of snapshots, which is typically on the order of hundreds. The Lyapunov equations in (15) are of dimension n and directly solving these equations is prohibitive as solving a Lyapunov equation scales with $O(n^3)$ [43]. The product of Y^*X requires $O(m^2n)$ operations which scales linearly in n. The resulting matrix is only $m \times m$ and hence the singular value decomposition in (19) can be performed at a reasonable computational cost.

IV. Results and Discussion

The results section of this paper focuses on obtaining a low-order model for a two-turbine array shown in Fig. 3. The dynamic system (10) becomes a single-input-single-output system. In this two-turbine example, the downstream turbine is held constant at an optimal operating point. The single input in this scenario is the axial induction factor of the upstream turbine. The single output is the power measured at the downstream turbine. Fig. 4 shows computed mean streamwise velocity. The turbines are located at $5D$ and $10D$. The simulation used $N_x = 300$ points between $[0, 15D]$ in the streamwise x direction and $N_y = 100$ points between $[0, 5D]$ in the spanwise y direction. This yields a total of 30,000 grid points with two velocities (u, v) defined at every point resulting in 60,000 states. A direct application of the stand balanced truncation technique requires the solution of the Lyapunov equations in (15). This is computationally intractable for this system. The BPOD method is implemented to obtain a reduced order model that retains the input/output behavior of the system. In addition, the BPOD method is compared to the input/output model obtained when using only the POD modes of the forward system.

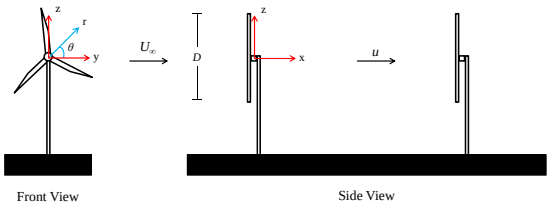

Fig. 3. Two Turbine Setup

We start by computing the POD modes of the forward system. Fig. 6 and 5 shows the computed POD modes for the actuator disk model. Note that modes 1 and 2 capture the low frequency, high energy structures in the model. The velocities are normalized by U_∞. Physically, when considering the flow behind the turbine, the lower POD modes correspond to larger frequency events such as large eddies generated in the wake of the turbine.

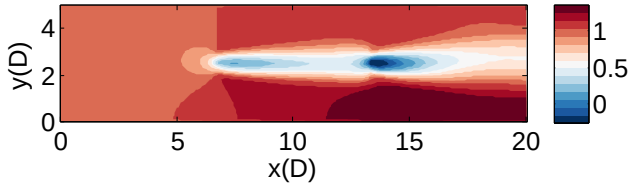

Fig. 4. Mean streamwise velocity computed using the actuator disk model

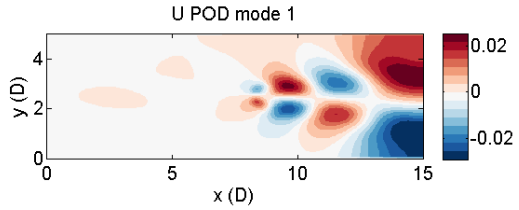

Fig. 5. Streamwise velocity POD mode 1

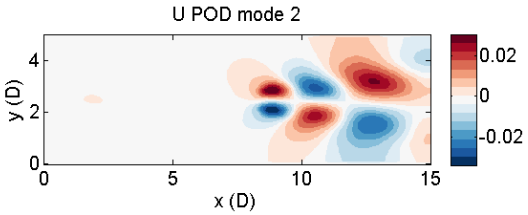

Fig. 6. Streamwise velocity POD mode 2

Using these POD modes and the Galerkin projection, described in Section III-A, the flow field can be reconstructed with relatively good agreement, see Fig. 7. For this example, 10 POD modes were used to reconstruct the flow. Again, this demonstrates that the POD modes are good at approximating specific snapshots of data.

Next, the BPOD modes were computed and the energy in the POD modes was compared to the energy in the BPOD modes. Fig. 8 shows that the percent of energy in the BPOD modes drops off faster than in the POD modes. This affects the way in which the reduced order models are constructed, i.e. fewer BPOD modes are needed to obtain a low-order input/output model.

Fig. 9 and 10 show the frequency response of the full order actuator disk model and the frequency response of the reduced order model constructed using POD and BPOD modes. Specifically, Fig. 9 shows the frequency response using 5 modes. The reduced order model using BPOD modes is better able to represent the frequency response with 5 modes than the reduced order model constructed using POD modes. As more modes are included in the reduced order model, the systems using POD and BPOD modes obtain the same frequency response. This highlights the benefit of using BPOD in that fewer modes are needed to represent the desired input/output response of the system.

Specifically, these BPOD modes provide a better representation of the input/output behavior than using only the POD modes for the forward system or the POD modes of the adjoint system. The forward system provides a representation

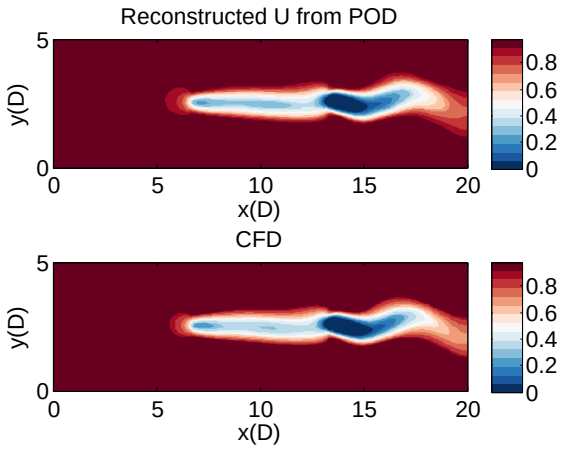

Fig. 7. Reconstructed flow using POD modes and the Galerkin projection.

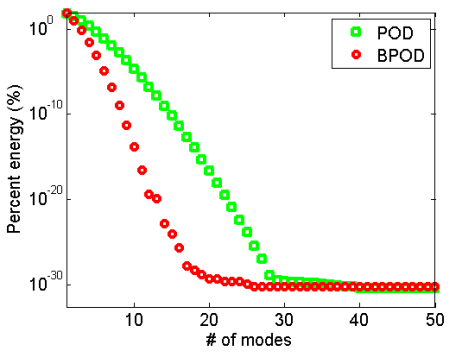

Fig. 8. Percentage of energy in each POD mode in the actuator disk model.

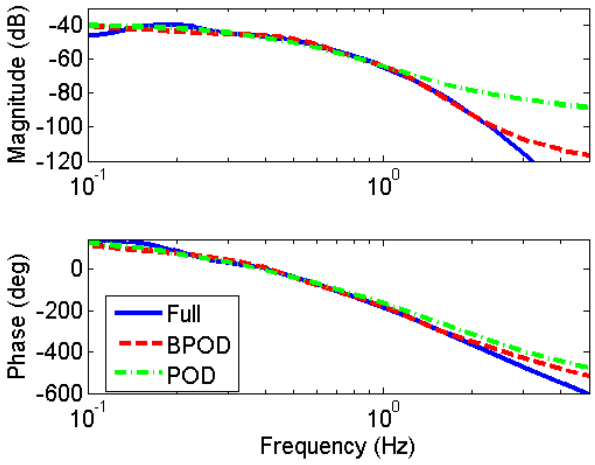

Fig. 9. Frequency response of the full order system and the reduced order system using 5 POD and 5 BPOD modes.

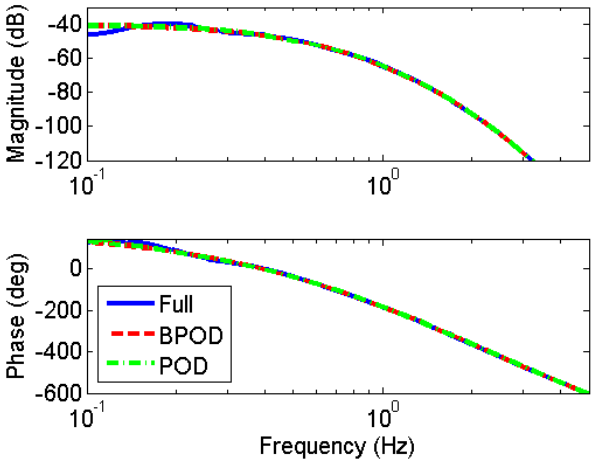

Fig. 10. Frequency response of the full order system and the reduced order system using 20 POD and 20 BPOD modes.

of the effects of specific inputs to the system. The adjoint system provides a representation of the effects due to a perturbation at the output of the system. By combining the information from the two systems, it is possible to say something about the input-to-output behavior of the whole system.

Note, there is a small, but noticeable mismatch between the reduced order models and the full order model at frequencies below 0.2 Hz in both Fig. 9 and 10. The accuracy of the reduced order models at these low frequencies can be improved by increasing the simulated time T_{max}. Specifically, these snapshots are collected over a certain time interval $[0, T_{max}]$. Thus very low frequencies are not captured by these snapshots, i.e. roughly frequencies below $\frac{1}{T_{max}}$ rad/s are not captured in the BPOD snapshots. The simulated time in this example is 10s. In addition, the sampling of snapshots from the simulation limits the high frequency component of the reduced order model. For this case, the sampling frequency was 10^{-4} and 1kHz is the highest frequency this model can capture. Thus the reduced order model provides a good input/output model for frequencies in this middle band.

V. Conclusions and Future Work

This paper used BPOD to develop a low-order model that can be used for wind farm control design and analysis. This approach takes advantage of characterizing the dominant dynamics in the flow and provides a low-order approximation of the flow. Using this low-order approximation, a reduced order model can be constructed that retains the input-to-output behavior seen in the full order model. This reduced order model has a low computational intensity and contains the necessary dynamics that are important for wind farm control.

Future work includes extending this model reduction technique to high-fidelity models, such as large-eddy simulations. In addition, preliminary wind farm controllers will be developed using these low-order models and validated in high-fidelity simulations and field tests.

VI. Acknowledgments

This work was supported by the National Science Foundation under Grant No. NSF-CMMI-1254129 entitled CAREER: Probabilistic Tools for High Reliability Monitoring and Control of Wind Farms. Any opinions, findings, and conclusions or recommendations expressed in this material are those of the authors and do not necessarily reflect the views of the NSF.

References

[1] R. Wiser, "Renewable portfolio standards in the united states - a status report with data through 2007," LBNL-154E, Lawerence Berkeley National Laboratory, 2008.

[2] L. P. Chamorro and F. Porté-Agel, "Turbulent flow inside and above a wind farm: a wind-tunnel study," *Energies*, vol. 4, no. 11, pp. 1916–1936, 2011.

[3] J. Hong, M. Toloui, L. P. Chamorro, M. Guala, K. Howard, S. Riley, J. Tucker, and F. Sotiropoulos, "Natural snowfall reveals large-scale flow structures in the wake of a 2.5-mw wind turbine," *Nature communications*, vol. 5, 2014.

[4] K. B. Howard, L. P. Chamorro, and M. Guala, "An experimental case study of complex topographic and atmospheric influences on wind turbine performance," in *51st AIAA Aerospace Sciences Meeting Including the New Horizons Forum and Aerospace Exposition (AIAA, 2013)*, 2013.

[5] E. Bitar and P. Seiler, "Coordinated control of a wind turbine array for power maximization," in *American Control Conference (ACC), 2013*, pp. 2898–2904, 2013.

[6] P. M. O. Gebraad, F. C. van Dam, and J. W. van Wingerden, "A model-free distributed approach for wind plant control," in *American Control Conference (ACC), 2013*, pp. 628–633, 2013.

[7] K. E. Johnson and G. Fritsch, "Assessment of extremum seeking control for wind farm energy production," *Wind Engineering*, vol. 36, no. 6, pp. 701–716, 2012.

[8] K. E. Johnson and N. Thomas, "Wind farm control: Addressing the aerodynamic interaction among wind turbines," in *American Control Conference*, pp. 2104–2109, 2009.

[9] J. R. Marden, S. Ruben, and L. Pao, "A model-free approach to wind farm control using game theoretic methods," *IEEE Transactions on Control Systems Technology*, pp. 1207–1214, 2013.

[10] J. Schepers and S. Van der Pijl, "Improved modelling of wake aerodynamics and assessment of new farm control strategies," in *Journal of Physics: Conference Series*, vol. 75 012039, IOP Publishing, 2007.

[11] L. Machielse, S. Barth, E. Bot, H. Hendriks, and G. Schepers, "Evaluation of heat and flux farm control - final report," ECN-E–07-105, Energy Research Centre of the Netherlands (ECN), 2007.

[12] N. O. Jensen, "A note on wind generator interaction," Tech. Rep. Risø-M-2411, Risø, 1983.

[13] J. F. Ainslie, "Calculating the flowfield in the wake of wind turbines," *Journal of Wind Engineering and Industrial Aerodynamics*, vol. 27, no. 1, pp. 213–224, 1988.

[14] M. Churchfield and S. Lee, "NWTC design codes-SOWFA," `http://wind.nrel.gov/designcodes/simulators/SOWFA`, 2012.

[15] X. Yang and F. Sotiropoulos, "On the predictive capabilities of les-actuator disk model in simulating turbulence past wind turbines and farms," in *American Control Conference*, pp. 2878–2883, 2013.

[16] K. Nilsson, S. Ivanell, K. S. Hansen, R. Mikkelsen, J. N. Sørensen, S.-P. Breton, and D. Henningson, "Large-eddy simulations of the lillgrund wind farm," *Wind Energy*, 2014.

[17] P. Holmes, J. L. Lumley, and G. Berkooz, *Turbulence, coherent structures, dynamical systems and symmetry*. Cambridge university press, 1998.

[18] M. Ilak, *Model reduction and feedback control of transitional channel flow*. PhD thesis, Princeton University, 2009.

[19] D. Bastine, B. Witha, M. Wächter, and J. Peinke, "Towards a simplified dynamic wake model using pod analysis," *arXiv preprint arXiv:1409.1150*, 2014.

[20] T. Burton, N. Jenkins, D. Sharpe, and E. Bossanyi, *Wind energy handbook*. John Wiley & Sons, 2011.

[21] L. Y. Pao and K. E. Johnson, "Control of wind turbines," *Control Systems, IEEE*, vol. 31, no. 2, pp. 44–62, 2011.

[22] P. Fleming, P. Gebraad, J.-W. van Wingerden, S. Lee, M. Churchfield, A. Scholbrock, J. Michalakes, K. Johnson, and P. Moriarty, "The SOWFA super-controller: A high-fidelity tool for evaluating wind plant control approaches," tech. rep., National Renewable Energy Laboratory (NREL), Golden, CO., 2013. Proceedings of the EWEA 2013.

[23] P. Fleming, P. Gebraad, M. Churchfield, S. Lee, K. Johnson, J. Michalakes, J.-W. van Wingerden, and P. Moriarty, "SOWFA + super controller user's manual," tech. rep., National Renewable Energy Laboratory (NREL), Golden, CO., 2013.

[24] J. N. Sørensen and A. Myken, "Unsteady actuator disc model for horizontal axis wind turbines," *Journal of Wind Engineering and Industrial Aerodynamics*, vol. 39, no. 1, pp. 139–149, 1992.

[25] J. N. Sørensen and C. W. Kock, "A model for unsteady rotor aerodynamics," *Journal of wind engineering and industrial aerodynamics*, vol. 58, no. 3, pp. 259–275, 1995.

[26] H. Schlichting, K. Gersten, and K. Gersten, *Boundary-layer theory*. Springer, 2000.

[27] K. E. Johnson, L. Y. Pao, M. J. Balas, and L. J. Fingersh, "Control of variable-speed wind turbines: standard and adaptive techniques for maximizing energy capture," *Control Systems, IEEE*, vol. 26, no. 3, pp. 70–81, 2006.

[28] O. Zikanov, *Essential computational fluid dynamics*. John Wiley & Sons, 2010.

[29] S. Wang and P. Seiler, "Gain scheduled active power control for wind turbines," in *AIAA Atmospheric Flight Mechanics Conference*, 2014.

[30] P. J. Schmid and D. S. Henningson, *Stability and transition in shear flows*, vol. 142. Springer, 2001.

[31] C. Rowley, "Model reduction for fluids, using balanced proper orthogonal decomposition," *International Journal of Bifurcation and Chaos*, vol. 15, no. 03, pp. 997–1013, 2005.

[32] K. Willcox and J. Peraire, "Balanced model reduction via the proper orthogonal decomposition," *AIAA journal*, vol. 40, no. 11, pp. 2323–2330, 2002.

[33] S. Lall, J. E. Marsden, and S. Glavaški, "A subspace approach to balanced truncation for model reduction of nonlinear control systems," *International journal of robust and nonlinear control*, vol. 12, no. 6, pp. 519–535, 2002.

[34] M. Balajewicz, *A New Approach to Model Order Reduction of the Navier-Stokes Equations*. PhD thesis, Duke University, 2012.

[35] B. Moore, "Principal component analysis in linear systems: Controllability, observability, and model reduction," *Automatic Control, IEEE Transactions on*, vol. 26, no. 1, pp. 17–32, 1981.

[36] L. Pernebo and L. Silverman, "Model reduction via balanced state space representations," *Automatic Control, IEEE Transactions on*, vol. 27, no. 2, pp. 382–387, 1982.

[37] D. F. Enns, "Model reduction with balanced realizations: An error bound and a frequency weighted generalization," in *Decision and Control, 1984. The 23rd IEEE Conference on*, vol. 23, pp. 127–132, IEEE, 1984.

[38] S. Skogestad and I. Postlethwaite, *Multivariable feedback control: analysis and design*, vol. 2. Wiley New York, 2007.

[39] A. Jameson, "Aerodynamic shape optimization using the adjoint method," *Lectures at the Von Karman Institute, Brussels*, 2003.

[40] M. B. Giles and N. A. Pierce, "An introduction to the adjoint approach to design," *Flow, turbulence and combustion*, vol. 65, no. 3-4, pp. 393–415, 2000.

[41] P. Luchini and A. Bottaro, "Adjoint equations in stability analysis," *Annual Review of Fluid Mechanics*, vol. 46, no. 1, p. 493, 2014.

[42] C. Wunsch, *Discrete inverse and state estimation problems: with geophysical fluid applications*, vol. 2. Cambridge University Press Cambridge, 2006.

[43] R. H. Bartels and G. Stewart, "Solution of the matrix equation ax+ xb= c [f4]," *Communications of the ACM*, vol. 15, no. 9, pp. 820–826, 1972.